Geomech. Geophys. Geo-energ. Geo-resour. (2024) 10:32
https://doi.org/10.1007/s40948-024-00754-0

RESEARCH

Reasonable value range of damage stress during rock brittle failure under compression

Baicun Yang · Xinyu Jiang · Yongting Duan · Chuyang Song

Received: 21 October 2023 / Accepted: 13 January 2024

Abstract It is significant to clarify the reasonable value range of damage stress in the brittle failure process of rock to predict rock instability, such as collapse and landslide. Previous studies on damage stress were mostly limited to the statistical analysis of results obtained through laboratory rock mechanics experiments, and relevant theoretical studies are urgently needed. This study first derived the theoretical expression of the ratio of the rock damage stress to the peak stress σ_{cd}/σ_f by combining the three dimensional renormalization group model established by the proper stress transfer mechanism with the rock damage constitutive model, and obtained its theoretical range. Then, the rationality of the theoretical results was tested by analyzing the statistical results obtained through laboratory rock mechanics experiments for samples with different lithologies under different confining pressures. The reasonable value range of σ_{cd}/σ_f for describing the brittle failure of rock under compression is [0.76, 0.93]. The reasons for some experimentally obtained σ_{cd}/σ_f values falling outside of the reasonable range are discussed. The findings of this study can be useful for the investigation of disaster mechanisms and the development of rock mass instability prediction models.

Article highlights

1. A three-dimensional renormalization group model of the brittle failure of rock was established.
2. Reasonable ratio range between damage stress and peak stress during rock brittle failure was derived in theory.
3. The reasonable ratio range was tested by 470 sets of laboratory rock mechanics experimental data.

Keywords Brittle failure · Damage stress · Peak stress · Renormalization group theory · Stress transfer mechanism

Supplementary Information The online version contains supplementary material available at https://doi.org/10.1007/s40948-024-00754-0.

B. Yang (✉) · X. Jiang · C. Song
School of Resources and Civil Engineering, Northeastern University, Shenyang 110819, People's Republic of China
e-mail: yangbaicun@mail.neu.edu.cn

Y. Duan
Key Laboratory of Ministry of Education On Safe Mining of Deep Metal Mines, Northeastern University, Shenyang 110819, People's Republic of China

Y. Duan
Key Laboratory of Liaoning Province On Deep Engineering and Intelligent Technology, Northeastern University, Shenyang 110819, People's Republic of China

Published online: 27 January 2024

1 Introduction

Elucidating the mechanical behavior characteristics of the brittle failure of rock under uniaxial or triaxial compression is essential for revealing the disaster mechanism of rock instability and predicting rock instability such as collapse and landslide (Peng et al. 2013a, b; Kong et al. 2018; Liu et al. 2019; Geng and Cao 2020; Yang et al. 2022a; Wang et al. 2022, 2023). Numerous studies (Bieniawski 1967; Martin 1997; Cai et al. 2004; Xue et al. 2014b; Taheri et al. 2020; Liu et al. 2022) have shown that the evolution of the deformation damage of rock under uniaxial or triaxial compression can be divided into five stages, namely, the crack closure, elastic region, stable crack growth, unstable crack growth, and onset of post peak region; the corresponding stress thresholds are the crack closure stress (σ_{cc}), crack initiation stress (σ_{ci}), crack damage stress (σ_{cd}), and peak stress (σ_f) (Fig. 1). As a stress threshold, σ_{cd} has been widely used in rock mass engineering practice in different ways: (1) as an effective indicator for characterizing the long-term strength of rock mass, and for predicting and evaluating the long-term stability of rock mass engineering, such as tunnel and slope engineering (Martin and Chandler 1994; Cai et al. 2004; Chandler 2013; Kong et al. 2018); (2) as an effective parameter for calculating rock burst proneness, and assessing the rock burst risk of underground rock mass (He et al. 2010; Chen et al. 2014; Zhang et al. 2017; Li and Zhou 2018).

Over the years, many studies have investigated the range of σ_{cd} values. Based on Griffith's theory and results obtained through multiaxial compression experiments on norite samples, Bieniawski (1967) reported that σ_{cd} is approximately 0.8 times equal to σ_f in the brittle failure of rock. Martin and Chandler (1994) conducted uniaxial and triaxial compression experiments on granite, and reported that the σ_{cd} value was related to rock damage accumulation; the value of σ_{cd}/σ_f ranged from 0.7 to 0.9. Katz and Reches (2004) conducted macroscopic mechanics experiments and made microscopic crack observations to analyze the rock damage and failure mechanisms under triaxial compression. They reported that spontaneous rock failure occurred near the stress threshold of $0.95\sigma_f$. Ranjith et al. (2010) investigated the effect of CO_2 adsorption on the σ_{cd} value of coal based on acoustic emission detection technology, and found that the increase of CO_2 saturation led to the decrease of σ_{cd}/σ_f. Xue et al. (2014a) analyzed the statistical results obtained through 251 sets of uniaxial compression experiments on rock samples, and found that the σ_{cd}/σ_f values of low porosity magmatic rock, sedimentary rock, and metamorphic rock were 0.78 ($\pm$0.11), 0.85 ($\pm$0.11), and 0.73 ($\pm$0.18), respectively. Ning et al. (2017) proposed a method for determining σ_{cd} based on the energy dissipation principle, and calculated the σ_{cd}/σ_f of coal under triaxial compression conditions as 0.8087–0.8677. Pepe et al. (2017) analyzed the main physical and mechanical parameters of 480 sets of rock samples and

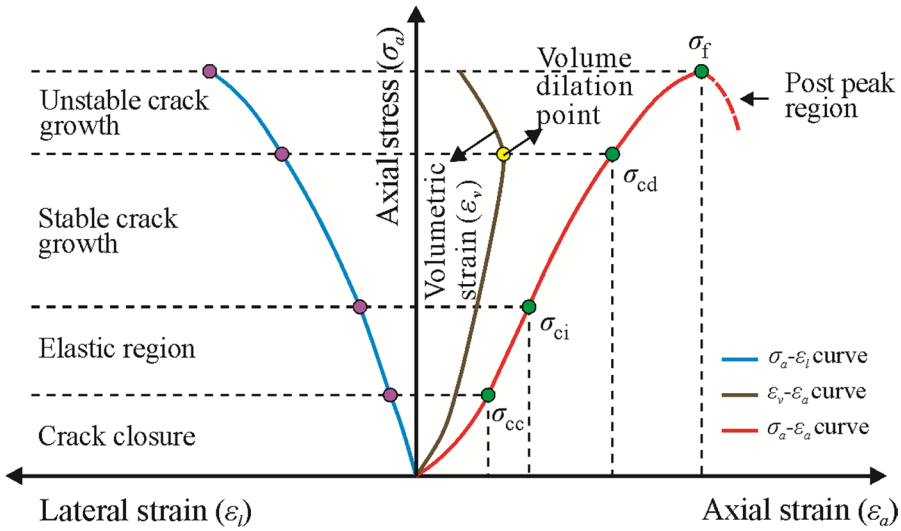

Fig. 1 Schematic diagram of stress–strain curve during brittle failure of rock under compression

established equations for predicting σ_{cd}. Peng et al. (2018) surveyed 926 sets of uniaxial and triaxial compression test data and obtained the distribution range of σ_{cd}/σ_f for rock brittle failure under compression conditions within a relatively small range. Li et al. (2020) conducted granite compression experiments using the GB-FDEM method, and found that the end-friction, slenderness ratio, loading rate, and confining pressure greatly affect the σ_{cd} and σ_f values, while the impact on the range of σ_{cd}/σ_f is small. Previous studies have enriched our understanding of the reasonable range of σ_{cd}/σ_f and clarified that the range of σ_{cd}/σ_f is relatively small. However, previous methods have mainly relied on laboratory rock mechanics experiments to analyze the range of σ_{cd}/σ_f values based on statistics and the analysis of the results obtained through uniaxial or triaxial compression tests on a limited number and certain types of rock samples at specific sampling locations. Owing to limitations related to the sampling locations, lithology, and sample quantities, the reasonable range of σ_{cd}/σ_f values remains unclear. Therefore, relevant theoretical studies are urgently needed.

This study used the renormalization group model and the rock damage constitutive model to derive the reasonable range of σ_{cd}/σ_f values. Then, the rationality of the theoretical derivation results was confirmed through laboratory rock mechanics tests at different locations with different lithologies and confining pressure. The findings of this study have significant practical implications for rock mass engineering.

2 Theoretical study on reasonable range of σ_{cd}/σ_f values

Essentially, the brittle failure process of rocks under compression is the evolution of damage, from local damage to complete failure, caused by stress. This process can be studied using percolation theory (Otsuka 1972; Shao and He 2001; Alkan 2009; Liu and Regenauer-Lieb 2021; Lv et al. 2022). Percolation theory explains that the properties of a system undergo a sharp change at a critical point, leading to a transformation of some form of long-range correlation (Broadbent and Hammersley 1957). This sudden change of long-range system correlation is called percolation transition, and the threshold corresponding to the percolation transition is called the percolation threshold. Previous studies have shown that, when rock damage accumulates to σ_{cd}, the long-range system correlation suddenly changes, resulting in the spontaneous evolution of rock failure instability under constant external loading. Therefore, the rock damage value corresponding to σ_{cd} is the system's percolation threshold (Qin et al. 2010; Xue et al. 2013; Lv et al. 2022). Further research (Sahimi 1996; Guéguen et al. 1997) found that physical systems at the critical state near the percolation threshold have infinite freedom, which is difficult to describe using traditional mathematical methods. The renormalization group method (Chen et al. 2002; Hristopulos 2003; Yang et al. 2022a) uses the scale-invariant property of the rock system at the percolation threshold to calculate the critical failure probability, which is an effective method for studying percolation problems.

The essence of renormalization group theory is upscaling, which involves changing the scale of the investigated object to emphasize a certain physical quantity that remains invariant at the percolation threshold, thus revealing its governing law (Hristopulos 2003; Wei et al. 2019; Xie et al. 2023). This approach has been widely used in studies investigating critical phenomena of rock damage evolution (Shao et al. 2009; Xue et al. 2014b; Pan and Lü 2018). Therefore, this study used the renormalization group method to derive the reasonable range of σ_{cd}/σ_f.

2.1 3D renormalization process

Numerous studies (Qin et al. 2010; Huang 2012; Chen et al. 2021; Dong et al. 2021; Yang et al. 2022b) have shown that a locked segment is a large-scale slab-shaped rock structure along a potential slip surface in a locked-segment-type slope to resist instability, which is a key geological structure subjected to stress concentration and dominant slope stability. As shown in Fig. 2, the locked segment was divided into n levels of cubic blocks, each block comprising eight lower-level blocks, and each second-level block comprising eight first-level blocks. The locked segment is the $n+1$ level block, which comprises eight n level blocks. Based on the scale invariance characteristics near the critical threshold of renormalization group theory, the general rules around σ_{cd} can be determined by investigating the failure probability of arbitrary scale blocks. Therefore, this study first investigated the relationship between the failure probability of the

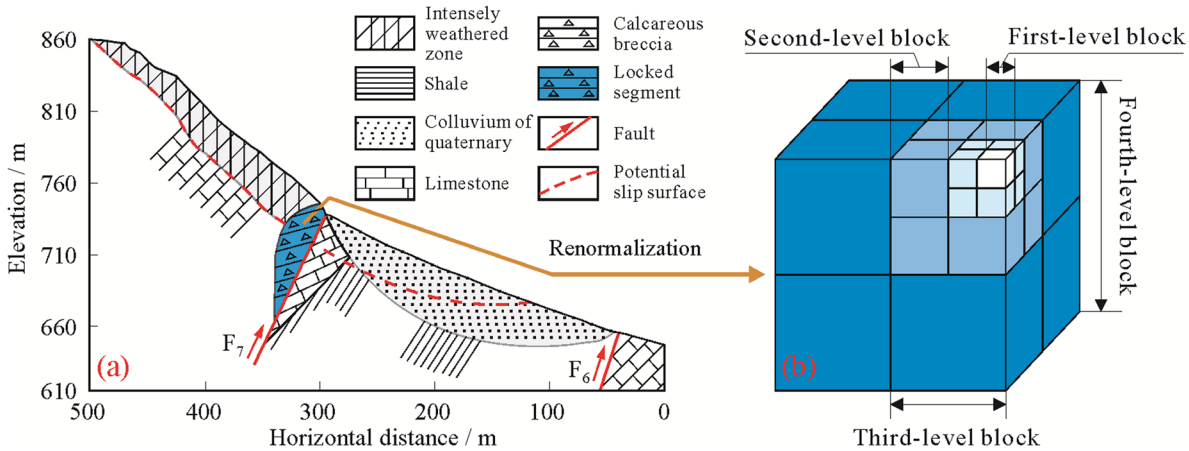

Fig. 2 **a** Geological profile of typical locked-segment-type slope; **b** 3D renormalization group schematic of locked segment

second and first-level blocks to establish a connection between the $n+1$ and n level blocks.

It is assumed that the failure criterion of a second-level block in the renormalization group model is that all its first-level blocks break (Xue et al. 2014b; Yang et al. 2022a). Figure 3 shows all possible combinations for second-level block failure (where b represents a broken block and u represents an unbroken block). Considering b3u5 as an example, there are three broken first-level blocks and five unbroken first-level blocks in the second-level block. Depending on the spatial locations of the broken and unbroken blocks, b3u5 can be further divided into three subcases, namely, b3u5-1, b3u5-2, and b3u5-3. Except for b0u8 in Fig. 3, all other combinations of first-level broken and unbroken blocks can cause second-level block failure, as a result of the stress transfer among them. Therefore, the stress transfer mechanism between the first-level blocks must be clarified before calculating the critical failure probability of a second-level block.

2.2 Stress transfer mechanism

Yang et al. (2022a) proposed a new stress transfer mechanism between blocks in the renormalization group model, where the stress borne by a block is only proportionally transferred to the coplanar adjacent blocks. This mechanism has been successfully applied to in-situ direct shear experiment of rock mass and slope instability evolution. On this basis, this study extended the stress transfer mechanism between two-dimensional blocks to three-dimensional blocks, and the following stress transfer mechanism is proposed.

(1) When a block fails, the stress it bears is proportionally transferred to the coplanar adjacent blocks; otherwise, it is not transferred to other blocks. In the b1u7 case shown in Fig. 4a, the eight first-level blocks are labeled A, B, C, D, a, b, c, and d. The stress borne by the broken block B is proportionally transferred to the coplanar adjacent blocks A, C, and b.
(2) The broken block does not have bearing capacity, but can be used as a stress transfer path between blocks. For case b2u6-1 in Fig. 4b, the stresses borne by block B are proportionally transferred to the coplanar adjacent blocks A and C, and to blocks a and c that are coplanar with the broken block b.
(3) Failure occurs when all lower-level blocks constituting that block are broken.

A three-dimensional renormalization group model can be established by combining the possible failure combinations shown in Fig. 3 with the stress transfer mechanism between the blocks is shown in Fig. 4.

2.3 Unstable fixed point solution method

Assuming that the strength of the first-level block in the renormalization group model conforms to the

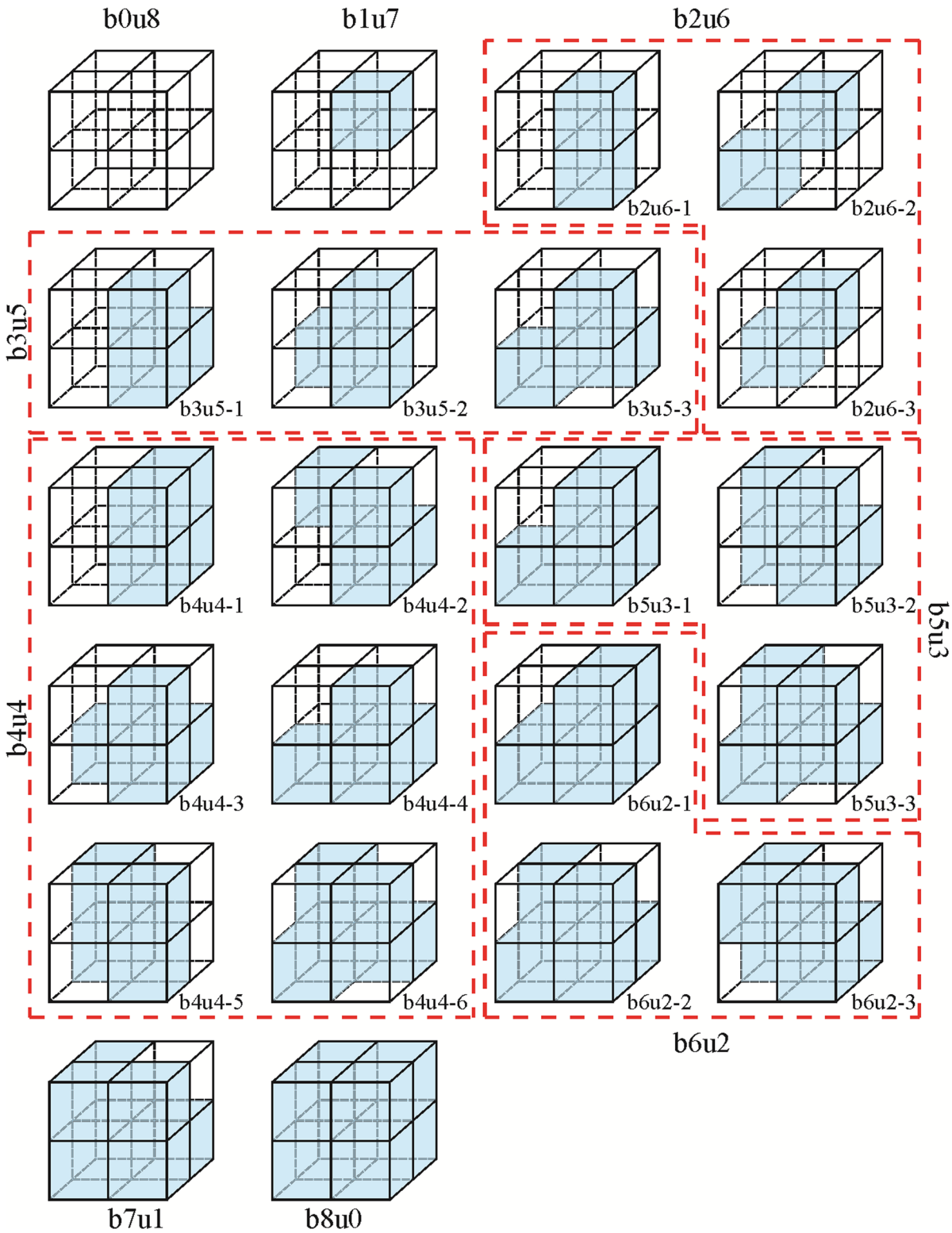

Fig. 3 Possible combinations for second-level block failure: blue blocks are broken blocks and white blocks are unbroken blocks

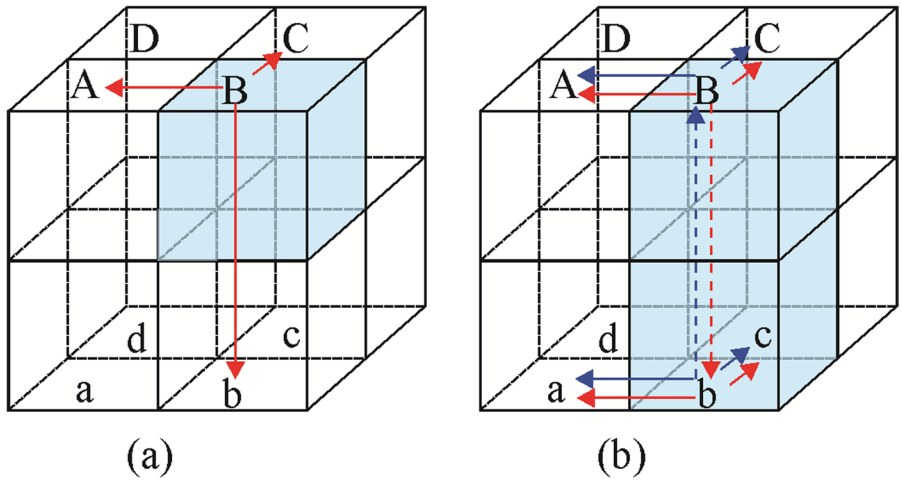

Fig. 4 Illustration of stress transfer mechanism between blocks: **a** case b1u7; **b** case b2u6-1. The red arrows indicate the stress transfer paths of the broken block B; the blue arrows indicate the stress transfer paths of the broken block b

Weibull distribution (Weibull 1951), the failure probability (P_α) can be expressed as follows:

$$P_\alpha = P\left(\sigma_f' < \alpha\sigma\right) = 1 - e^{\left[-\left(\frac{\alpha\sigma}{\sigma_0}\right)^m\right]} \tag{1}$$

where σ_f' is the strength of the micro-element, α is a scaling coefficient, σ is the stress of the micro-element, σ_0 is the statistical mean stress of the micro-element, and m is the Weibull shape parameter.

When α is equal to 1, Eq. (1) can be written as follows:

$$P_1 = P\left(\sigma_f' < \sigma\right) = 1 - e^{\left[-\left(\frac{\sigma}{\sigma_0}\right)^m\right]} \tag{2}$$

where P_1 is the probability of the block breaking when σ_f' is less than σ.

By combining Eqs. (1) and (2), the following equation is obtained:

$$P_\alpha = 1 - \left(1 - P_1\right)^{\alpha^m} \tag{3}$$

The flowing conditional probability $P_{e,f}$, which represents the probability of an unbroken block with local stress $f\sigma$ failing under an additional stress $(e-f)\sigma$ transmitted from another broken block, is expressed as follows:

$$P_{e,f} = \frac{P\left(f\sigma < \sigma_f' < e\sigma\right)}{P\left(\sigma_f' > f\sigma\right)} = \frac{P_e - P_f}{1 - P_f} \tag{4}$$

where e and f are scale parameters, P_e is the probability of the block breaking when σ_f' is less than $e\sigma$, and P_f is the probability of the block breaking when σ_f' is less than $f\sigma$.

As shown in Fig. 3, there are 21 possible combinations that can cause second-level block failure; therefore the failure probability of a second-level block, $P^{(2)}$, can be expressed as follows:

$$\begin{aligned} P^{(2)} = {} & P_{\text{b1u7}} + P_{\text{b2u6 - 1}} + P_{\text{b2u6 - 2}} + P_{\text{b2u6 - 3}} + P_{\text{b3u5 - 1}} + P_{\text{b3u5 - 2}} + P_{\text{b3u5 - 3}} \\ & + P_{\text{b4u4 - 1}} + P_{\text{b4u4 - 2}} + P_{\text{b4u4 - 3}} + P_{\text{b4u4 - 4}} + P_{\text{b4u4 - 5}} + P_{\text{b4u4 - 6}} + P_{\text{b5u3 - 1}} \\ & + P_{\text{b5u3 - 2}} + P_{\text{b5u3 - 3}} + P_{\text{b6u2 - 1}} + P_{\text{b6u2 - 2}} + P_{\text{b6u2 - 3}} + P_{\text{b7u1}} + P_{\text{b8u0}} \end{aligned} \tag{5}$$

where P_{b1u7} is the failure probability for the b1u7 case, $P_{\text{b2u6-1}}$ is the failure probability for the b2u6-1 case, $P_{\text{b2u6-2}}$ is the failure probability for the b2u6-2 case, $P_{\text{b2u6-3}}$ is the failure probability for the b2u6-3 case, $P_{\text{b3u5-1}}$ is the failure probability for the b3u5-1 case, $P_{\text{b3u5-2}}$ is the failure probability for the b3u5-2 case, $P_{\text{b3u5-3}}$ is the failure probability for the b3u5-3 case, $P_{\text{b4u4-1}}$ is the failure probability for the b4u4-1 case, $P_{\text{b4u4-2}}$ is the failure probability for the b4u4-2 case, $P_{\text{b4u4-3}}$ is the failure probability for the b4u4-3 case, $P_{\text{b4u4-4}}$ is the failure probability for the b4u4-4 case, $P_{\text{b4u4-5}}$ is the failure probability for the b4u4-5 case, $P_{\text{b4u4-6}}$ is the failure probability for the b4u4-6 case, $P_{\text{b5u3-1}}$ is the failure probability for the b5u3-1 case, $P_{\text{b5u3-2}}$ is the failure probability for the b5u3-2

case, $P_{b5u3\text{-}3}$ is the failure probability for the b5u3-3 case, $P_{b6u2\text{-}1}$ is the failure probability for the b6u2-1 case, $P_{b6u2\text{-}2}$ is the failure probability for the b6u2-2 case, $P_{b6u2\text{-}3}$ is the failure probability for the b6u2-3 case, P_{b7u1} is the failure probability for the b7u1 case, P_{b8u0} is the failure probability for the b8u0 case.

Figure 5 shows the process of deriving the failure probability for $P_{b3u5\text{-}1}$. As shown in Fig. 5, the three broken blocks are B, b, and c, and the stresses they bear are proportionally transferred to the four blocks A, C, a, and d that are coplanar with them, such that they all bear $7/4\sigma$ stresses. The unbroken blocks A, C, and d, and the broken block a are considered as an example to explain the stress transfer process between blocks. After block a fails, the stress is transferred to blocks A, C, and d and each block is subjected to $7/3\sigma$ stress. Then, there are three cases of second-level block failure being triggered as follows: 1) the A, C, and d blocks break, the stress is transferred to block D and causes its failure; 2) the A and C blocks break, the d block does not break, and the stress is transferred to the D and d blocks and causes them to bear $10/3\sigma$ and $14/3\sigma$ stresses, respectively. Next, the D and d blocks break simultaneously, or either block D or d breaks, and the stress is transferred to the other block and causes it to break; 3) the A block breaks, and stress is transferred to the C, D, and d blocks and makes them bear $28/9\sigma$, $16/9\sigma$, and $28/9\sigma$ stresses, respectively. If any of these three blocks break, the stress will be transferred to the remaining unbroken blocks, and a combination of the following cases will exist: 1) the C, D, and d blocks break; 2) the C and D blocks break and the d block does not break, and the stress is transferred to the d block and causes it to break, or the D and d blocks break and the C block does not break, and the stress is transferred to the C block and causes it to break; 3) the C and d blocks break and the D block does not break, and the stress is transferred to the D block and causes it to break; 4) the C block breaks, the D and d blocks do not break, and the stress is transferred to blocks D and d and causes them to bear $10/3\sigma$ and $14/3\sigma$ stresses, respectively; after the end of this round of stress transfer, the D and d blocks break simultaneously, or either block D or d breaks and the stress is transferred to the other block and causes it to break (consistent with block d breaking and blocks C and D not breaking); (5) the D block breaks, the C and d blocks do not break, and the stress is transferred to the C and d blocks and causes them to bear 4σ stresses; after the end of this round of stress transfer, the C and d blocks break simultaneously, or either block C or d breaks and the stress is transferred to the other block and causes it to break.

Using the method described above, a total of 1596 possible combinations causing second-level block fracture were calculated, and the expression of $P^{(2)}$ was obtained after substitution into Eq. (5), as follows:

$$P^{(2)} = f\left(P^{(1)}\right) \tag{6}$$

where $P^{(1)}$ is the failure probability of a first-level block, which is equal to P_1. Additional file 1: Appendix 1 shows the equation between $P^{(2)}$ and $P^{(1)}$.

By extending Eq. (6) to n level blocks, the following equation is obtained:

$$P^{(n+1)} = f\left(P^{(n)}\right) \tag{7}$$

where $P^{(n+1)}$ is the $n+1$ level block failure probability, and $P^{(n)}$ is the n level block failure probability. The specific details of the equation are given in Additional file 1: Appendix 2, and it can be seen that Eq. (7) is only related to the value of m.

Considering that renormalization group theory has scale invariance characteristics near the critical threshold, the following equation can be established:

$$P^{(n)} = P^{(n+1)} \tag{8}$$

By combining Eqs. (7) and (8), the values of the unstable fixed points (P^*) corresponding to different m values can be calculated.

As shown in Fig. 6, the curves $P^{(n+1)} = f(P^{(n)})$ and $P^{(n)} = P^{(n+1)}$ have three intersection points, where 0 and 1 are stable fixed points and P^* is an unstable fixed point.

Yang et al. (2021) proposed that the reasonable range limit of the m value for describing the brittle failure behavior of rock is [1, 6] by establishing the quantitative relationship between the Weibull shape parameter and the fractal dimension of crack distribution for a stressed rock. By fitting the P^* values calculated in Fig. 6, the relationship between m and P^* can be obtained as follows (Fig. 7):

$$P^* = 0.659\mathrm{e}^{-0.7879m} + 0.049 \tag{9}$$

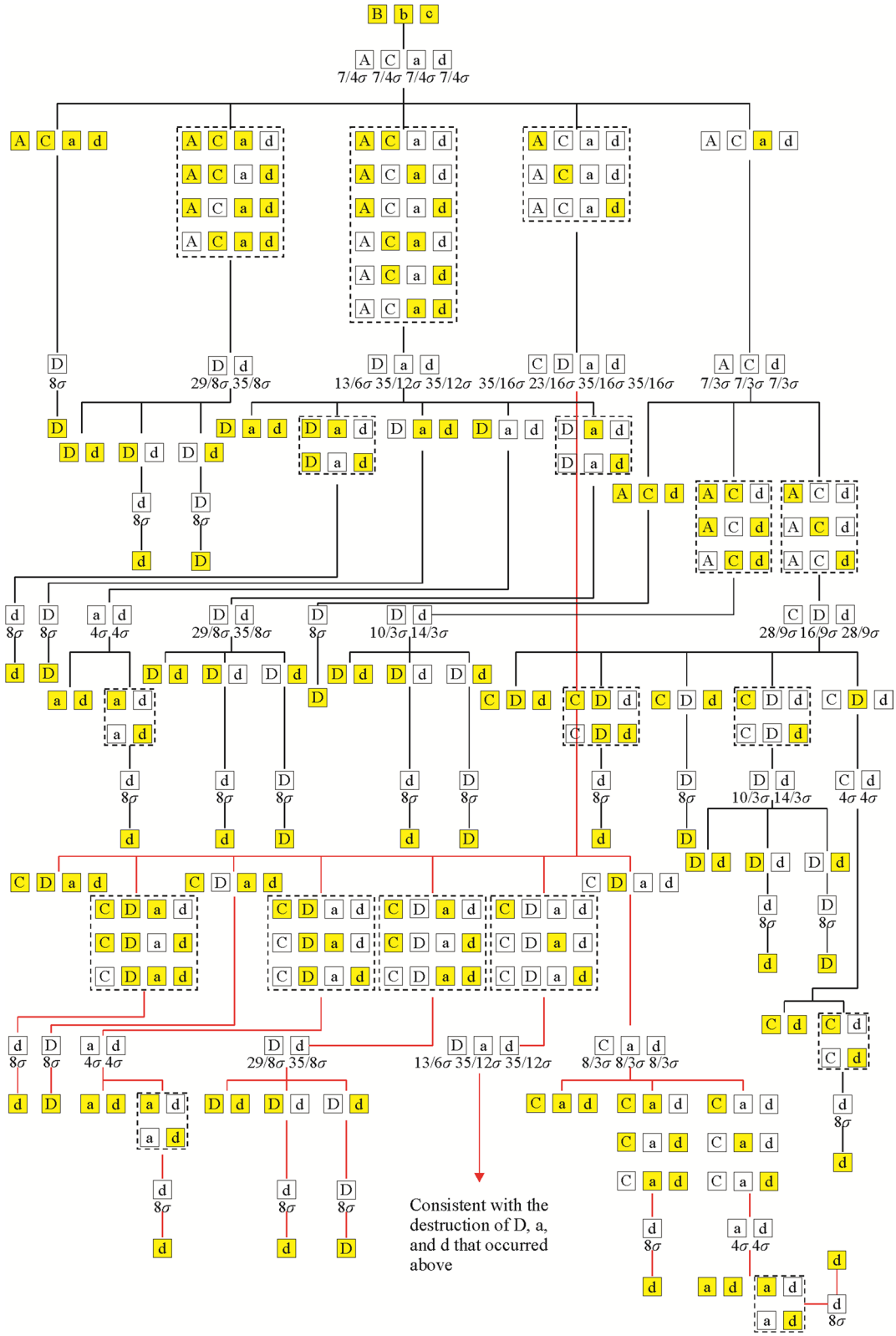
Consistent with the destruction of D, a, and d that occurred above

◂**Fig. 5** Schematic diagram of failure probability stress transfer in $P_{b3u5\text{-}1}$ case; the yellow boxes are broken blocks and the white boxes are unbroken blocks

2.4 Theoretical solutions for value range of σ_{cd}/σ_f

Qin et al. (2006) and Xue et al. (2013) proposed that the failure probability P_1 in the renormalization group model is expressed as follows:

$$P_1 = 1 - e^{\left[-\left(\frac{\varepsilon}{\varepsilon_0}\right)^m\right]} \tag{10}$$

where ε is the strain of the micro-element, and ε_0 is the statistical mean strain of the micro-element.

By substituting Eq. (9) into Eq. (10), the following equation is obtained:

$$\frac{\varepsilon_{cd}}{\varepsilon_0} = \left[-\ln(1-P^*)\right]^{\frac{1}{m}} \tag{11}$$

where ε_{cd} is the strain at σ_{cd}.

By combining the Weibull distribution and the damage constitutive model, Lemaitre (1984) proposed the following rock damage constitutive model:

$$\sigma = E\varepsilon e^{\left[-\left(\frac{\varepsilon}{\varepsilon_0}\right)^m\right]} \tag{12}$$

where E is the elastic modulus.

Considering that the first-order derivative of the stress–strain curve at the peak stress point during the brittle failure of rock is zero, the first-order derivative of Eq. (12) with respect to ε is as follows:

$$\frac{\varepsilon_f}{\varepsilon_0} = \left(\frac{1}{m}\right)^{\frac{1}{m}} \tag{13}$$

where ε_f is the strain at σ_f.

By substituting Eqs. (11) and (13) into Eq. (12), the following equation is obtained:

$$\frac{\sigma_{cd}}{\sigma_f} = \frac{\varepsilon_{cd}}{\varepsilon_f}(1-P^*)e^{\frac{1}{m}} = \left[-m\ln(1-P^*)\right]^{\frac{1}{m}}(1-P^*)e^{\frac{1}{m}} \tag{14}$$

As shown in Fig. 8, the value range of σ_{cd}/σ_f obtained from Eq. (14) is [0.76, 0.93] when m is [1, 6]. Hence, the theoretical solution for the reasonable value range of σ_{cd}/σ_f in the brittle failure of rock under compression is [0.76, 0.93].

3 Experimental investigation of reasonable range of σ_{cd}/σ_f values

To confirm the rationality of the theoretical solution, 470 sets of uniaxial compression and triaxial compression experimental data for magmatic, sedimentary, and metamorphic rocks were collected from previous studies. Specifically, 178 datasets for magmatic rocks, 104 datasets for sedimentary rocks, and 188 datasets for metamorphic rocks were collected (Table 1). The methods for determining σ_{cd} in Table 1 include the crack volumetric strains method (CVS; Martin and Chandler 1994), lateral strain response method (LSR; Nicksiar and Martin 2012), moving

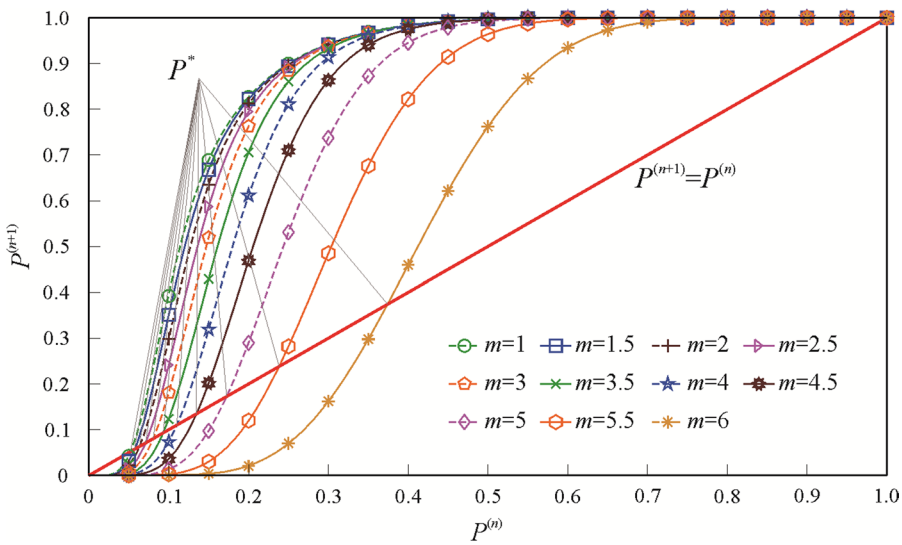

Fig. 6 Relationship between $P^{(n)}$, $P^{(n+1)}$, and P^* for different m values based on 3D renormalization group theory

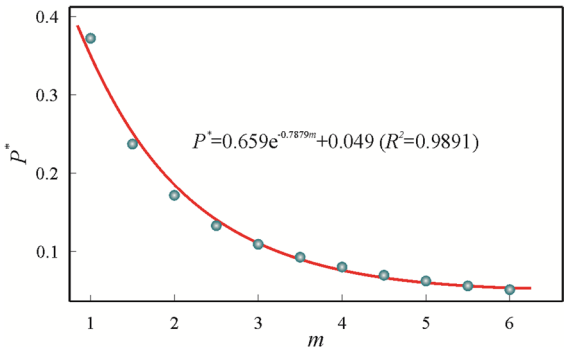

Fig. 7 Relationship between P^* value and m value

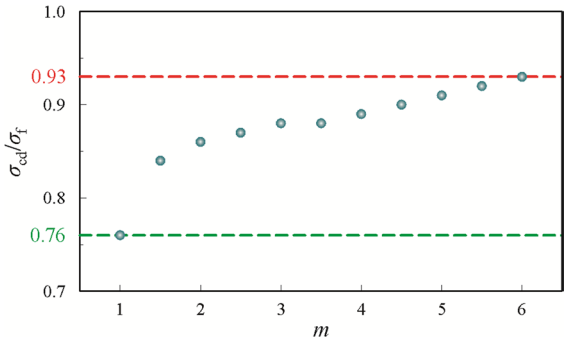

Fig. 8 Relationship between σ_{cd}/σ_f values and m values

point regression technique (MPR; Eberhardt et al. 1998), and acoustic emission method (AE; Ranjith et al. 2010).

Based on the experimental data in Table 1, the σ_{cd}/σ_f values were calculated for rock samples with different lithologies under different confining pressure (Fig. 9). As can be seen, most σ_{cd}/σ_f values lie in the range of [0.76, 0.93], which is consistent with the theoretical results. The mean value of σ_{cd}/σ_f for all rock samples is 0.83, and the mean values of σ_{cd}/σ_f for the magmatic, sedimentary, and metamorphic rocks are 0.82, 0.83, and 0.82, respectively, with variances of 0.0037, 0.0107, and 0.0058, respectively. Compared with the other two rock types, the range of the σ_{cd}/σ_f values of sedimentary rocks is more discrete, possibly owing to the rock anisotropy caused by the bedding structures of sedimentary rocks.

The plots in Figs. 10, 11, and 12 can be used to further analyze the range of σ_{cd}/σ_f values for the magmatic, sedimentary, and metamorphic rocks with different lithologies. The σ_{cd}/σ_f values for the magmatic rock specimens with different lithologies are shown in Fig. 10. As can be seen, the σ_{cd}/σ_f values of seven magmatic rocks, namely, granite, diorite, pegmatite, granodiorite, quartz monzodiorite, rhyolite, and tonalite, are mostly in the range of [0.76, 0.93], and the mean values are 0.82, 0.92, 0.77, 0.81, 0.82, 0.83, and 0.83, respectively. All mean values are within the theoretical range and confirm the rationality of the theoretical solution. The variance of σ_{cd}/σ_f for these seven magmatic rocks is 0.0034, 0.0030, 0.0045, 0.0048, 0.0017, 0.0012, and 0.0005, respectively. The variance of pegmatite and granodiorite is significantly larger compared with that of other rock samples, indicating that the range of σ_{cd}/σ_f for these two rocks has stronger discreteness.

Figure 11 shows the σ_{cd}/σ_f values of sedimentary rock samples with different lithologies. As can be seen, the σ_{cd}/σ_f values of the five sedimentary rocks, namely, sandstone, limestone, argillaceous limestone, calcareous shale, and shale, are mostly in the range of [0.76, 0.93], and the mean values are 0.88, 0.84, 0.77, 0.90, and 0.80, respectively. All mean values are within the range of the theoretical solutions, and confirm the rationality of the theoretical solutions. The σ_{cd}/σ_f variances of these five sedimentary rocks are 0.0050, 0.0118, 0.0078, 0.0050, and 0.0033, respectively. The variance of σ_{cd}/σ_f for limestone is significantly larger than that of other rock samples, indicating that its σ_{cd}/σ_f value is more discrete.

Figure 12 shows the σ_{cd}/σ_f values for the metamorphic rock samples with different lithologies. As can be seen, most data for the six metamorphic rocks, namely, marble, schist, coal, mica gneiss, amphibolite, and metagranite, are in the range of [0.76, 0.93], and the mean values are 0.83, 0.86, 0.81, 0.82, 0.80, and 0.83, respectively. All mean values are within the theoretical range, which confirms the rationality of the theoretical solutions. The σ_{cd}/σ_f variances of these metamorphic rocks are 0.0045, 0.0084, 0.0161, 0.0019, 0.0107, and 0.0039, respectively. Among them, the variances of σ_{cd}/σ_f for the coal and amphibolite rocks are significantly higher compared with the other rock samples, indicating that the σ_{cd}/σ_f range of the coal and amphibolite rocks is more discrete.

The plots in Figs. 13 and 14 can be used to further analyze the effect of different confining pressures on the range of σ_{cd}/σ_f values. The σ_{cd}/σ_f values of the rock samples under the confining pressures of

Table 1 Results of uniaxial and triaxial compression experiment for different rock types

No	Lithology	Site	Amount of data	Data sources	Determination method	Experimental type
1	Granite	Korea Hwangdeung	5	Chang and Lee (2004)	AE	Triaxial
2	Granite	Singapore	1	Ranjith et al. (2004)	AE	Uniaxial
3	Diorite	Sweden	7	Andersson et al. (2009)	CVS	Uniaxial
4	Pegmatite	Sweden	12	Nicksiar (2013)	LSR	Uniaxial
5	Granodiorite	Sweden	14	Nicksiar (2013)	LSR	Uniaxial
6	Tonalite	Sweden	9	Nicksiar (2013)	LSR	Uniaxial
7	Granite	Sweden	46	Nicksiar (2013)	LSR	Uniaxial
8	Granodiorite	Sweden	11	Nicksiar (2013)	LSR	Uniaxial
9	Quartz monzodiorite	Sweden	33	Nicksiar (2013)	LSR	Uniaxial
10	Rhyolite	Sweden	5	Nicksiar (2013)	LSR	Uniaxial
11	Granite	China	19	Wang et al. (2015)	LSR	Triaxial
12	Granite	China	1	Li and Zhou (2018)	LSR	Uniaxial
13	Granite	China	9	Zhou et al. (2019)	AE	Triaxial
14	Granite	China	6	You et al. (2021)	LSR	Triaxial
15	Sandstone	China	10	Peng et al. (2013b)	CVS	Triaxial
16	Argillaceous limestone	Canada	21	Nicksiar (2013)	LSR	Uniaxial
17	Calcareous Shale	Canada	4	Nicksiar (2013)	LSR	Uniaxial
18	Shale	Canada	6	Nicksiar (2013)	LSR	Uniaxial
19	Limestone	China	60	Zhao et al. (2021)	LSR	Triaxial
20	Sandstone	China	3	Liang et al. (2023)	CVS	Uniaxial
21	Coal	Australian	6	Ranjith et al. (2010)	AE	Uniaxial
22	Marble	China	18	Yang and Liu (2012)	LSR	Triaxial
23	Marble	China	17	Wang et al. (2012)	AE	Uniaxial
24	Mica gneiss	Finland	53	Nicksiar (2013)	LSR	Uniaxial
25	Amphibolite	America	6	Nicksiar (2013)	LSR	Uniaxial
26	Metagranite	Sweden	38	Nicksiar (2013)	LSR	Uniaxial
27	Marble	China	20	Zhang et al. (2016)	LSR/CVS	Triaxial
28	Coal	China	6	Ning et al. (2017)	\	Triaxial
29	Schist	China	9	Huang et al. (2021a)	LSR	Uniaxial
30	Coal	China	15	Hao et al. (2021)	MPR	Uniaxial

0 MPa, 5 MPa, 10 MPa, 15 MPa, 20 MPa, 25 MPa, 30 MPa, 35 MPa, and 40 MPa are mostly in the range of [0.76, 0.93]. The mean values are 0.82, 0.85, 0.84, 0.86, 0.83, 0.84, 0.80, 0.80, and 0.80, respectively, all of which are within the theoretical range, confirming the rationality of the theoretical solution. The variances of σ_{cd}/σ_f under different confining pressures are 0.0053, 0.0027, 0.0055, 0.0069, 0.0079, 0.0171, 0.0068, 0.0033, and 0.0027, respectively. For the confining pressure of 25 MPa, the variance is significantly higher compared with the other confining pressures, indicating that the range of the σ_{cd}/σ_f values under this confining pressure is more discrete.

In summary, most σ_{cd}/σ_f values in 470 sets of rock samples are in the range of [0.76, 0.93], and the mean values of σ_{cd}/σ_f for rocks with different lithologies under different confining pressure conditions are in the range of [0.76, 0.93]. The experimental results are consistent with the theoretical results, and reveal that the range of σ_{cd}/σ_f values for the brittle failure process of rock is [0.76, 0.93].

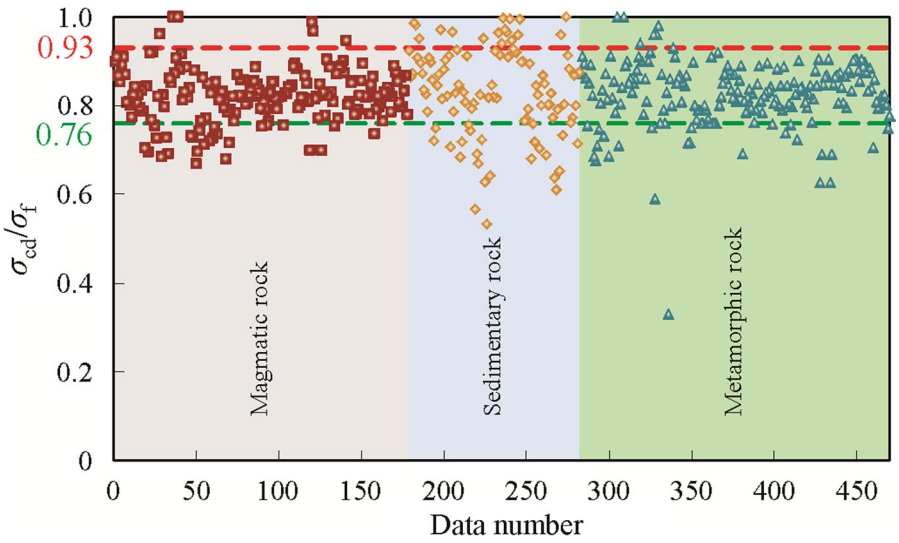

Fig. 9 σ_{cd}/σ_f values for different rock types

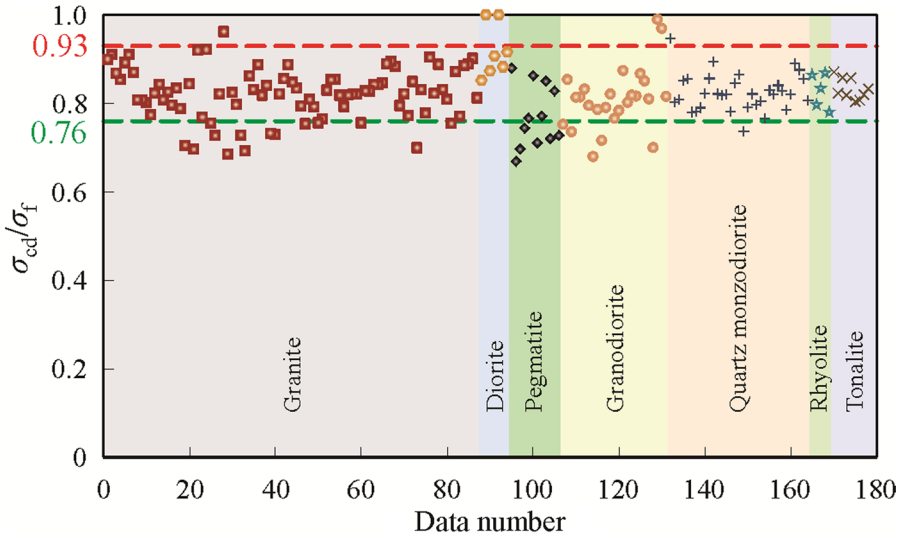

Fig. 10 σ_{cd}/σ_f values for magmatic rock samples with different lithologies

4 Discussion

Among the 470 sets of data collected in this study, most σ_{cd}/σ_f values are in the range of [0.76, 0.93], while individual data are not within this range. The reasons for this phenomenon are analyzed below.

(1) The m values of some rocks may fall outside of the range of [1, 6], owing to factors such as the rock properties and loading conditions. Yang et al. (2021) proposed that the reasonable value range for the m value is [1, 6] when the Weibull distribution is used to describe the brittle failure of rock. This range limit of the m value has been verified by a large number of experiments (Gao et al. 2020; Yang et al. 2021; Shi et al. 2023). On this basis, this study derived the reasonable value range of σ_{cd}/σ_f. Previous studies have shown that the rock properties (Maheshwari et al. 2009; Li et al. 2017; Zhang et al. 2022) and loading conditions such as the confining pressure (Cao and Zhang 2005; Cao et al. 2013; Yang et al. 2014; Huang et al. 2021b), loading rate (Yang et al. 2005; Nakamura et al. 2007; Cao et al. 2015; Li et al. 2023), and temperature (Jia et al. 2010; Yang et al. 2018; Pathiranagei and Gratchev 2022) can affect the m value during the brittle failure of rock. Under the influence of the above-mentioned factors, when the m value of

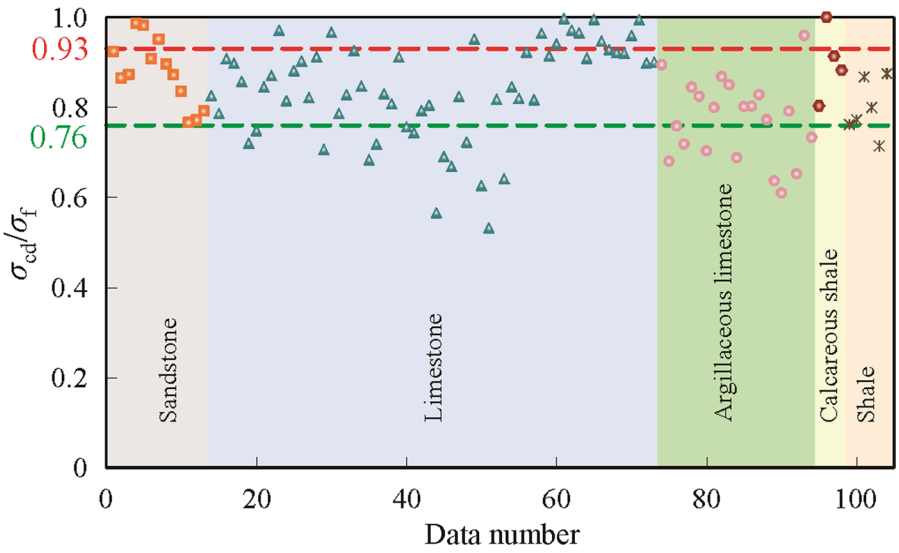

Fig. 11 σ_{cd}/σ_f values for sedimentary rock samples with different lithologies

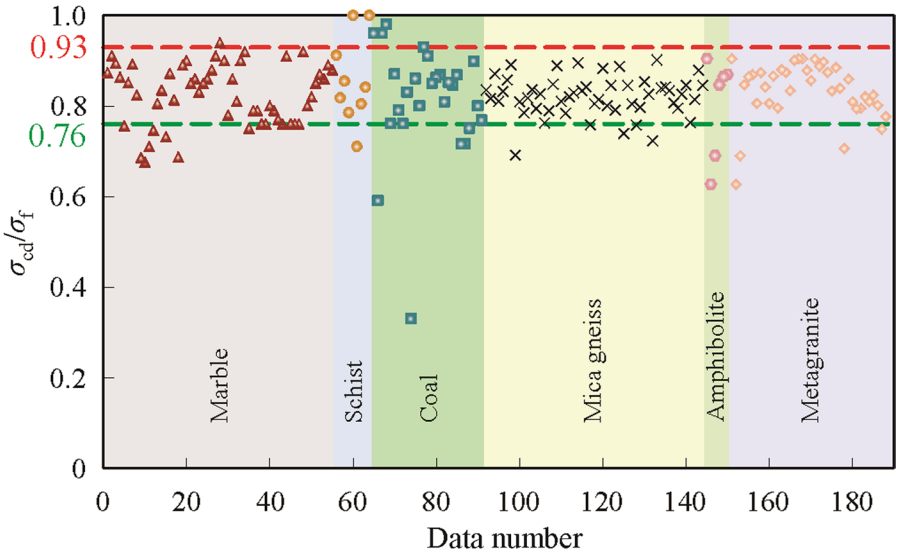

Fig. 12 σ_{cd}/σ_f values for metamorphic rock samples with different lithologies

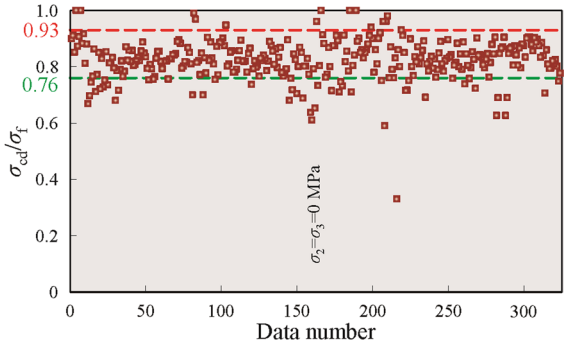

Fig. 13 σ_{cd}/σ_f values of different rock samples under uniaxial compression

rock samples is not in the range of [1, 6], the σ_{cd}/σ_f value may not be in the reasonable value range.

(2) The accuracy of the σ_{cd} values obtained through laboratory rock mechanics experiments is not satisfactory. Many methods, such as CVS, LSR, MPR, and AE, are used to determine the σ_{cd} values in laboratory uniaxial and triaxial compression experiments. As has been shown (Taheri et al. 2020; Zhang et al. 2020), widely disparate results may obtained when different methods are used to determine the σ_{cd} values of the same experimental data. Therefore, it is still difficult to determine the σ_{cd} value with satisfactory accuracy. For the

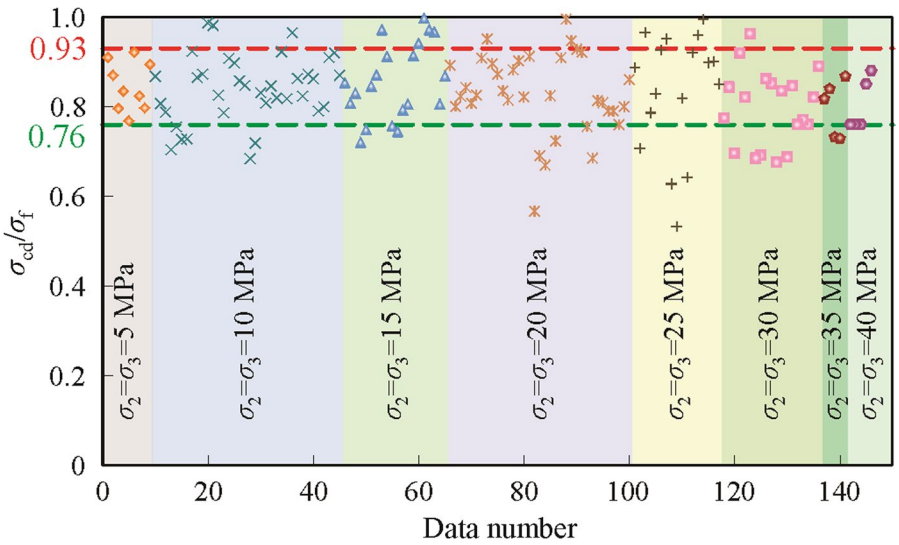

Fig. 14 σ_{cd}/σ_f values of different rock samples under triaxial compression

experimental data collected in this study, different methods for determining σ_{cd} were used, and the accuracy of individual experimental results needs to be verified. Therefore, it may result in the σ_{cd}/σ_f values not being in the reasonable range.

5 Conclusion

To determine the reasonable range of σ_{cd} during the brittle failure of rock under compression, the theoretical range of σ_{cd}/σ_f was derived by combining renormalization group theory and the rock damage constitutive model. Laboratory rock mechanics experiments with different lithologies under different confining pressures were collected to assess the rationality of the theoretical solution. The main conclusions drawn from this study are as follows:

(1) The stress transfer mechanism between the three-dimensional renormalization blocks was redefined, and a three-dimensional renormalization group model of the brittle failure of rock was established. By combining the renormalization group model and the rock damage constitutive model, the theoretical expression of σ_{cd}/σ_f was derived, and is only related to the m value in the Weibull distribution. According to the reasonable range of m values, the theoretical range of σ_{cd}/σ_f during the brittle failure of rock under compression was calculated as [0.76, 0.93].

(2) Data were obtained through 470 sets of rock mechanics experiments, and most σ_{cd}/σ_f values were in the range of [0.76, 0.93]. The mean σ_{cd}/σ_f values for rocks with different lithologies under different confining pressure were also in this range. The experimental results are consistent with the theoretical results, which confirms that the reasonable range of the σ_{cd}/σ_f values for the brittle failure of rock under compression is [0.76, 0.93].

(3) The reasons for some experimentally obtained σ_{cd}/σ_f values falling outside of the reasonable range were discussed. First, the m values of the samples were not within the reasonable range, owing to the rock properties and loading conditions. Second, the accuracy of the σ_{cd} values obtained through laboratory rock mechanics experiments must be confirmed.

Author Contributions Each author has contributed to this article. Xinyu Jiang derived the theoretical formula and collected the experimental data; Baicun Yang and Yongting Duan wrote this paper; Chuyang Song improved the paper's structure and language.

Funding This work was funded by the National Natural Science Foundation of China (42102309 and 42007243).

Availability of data and materials All the data is presented in the manuscript.

Declarations

Ethics approval Not applicable.

Consent for publication The authors agree with the publication of the manuscript.

Competing interests The authors declare no conflict of interest.

References

Alkan H (2009) Percolation model for dilatancy-induced permeability of the excavation damaged zone in rock salt. Int J Rock Mech Min Sci 46(4):716–724. https://doi.org/10.1016/j.ijrmms.2008.08.002

Andersson JC, Martin CD, Stille H (2009) The Äspö Pillar stability experiment: Part II—rock mass response to coupled excavation-induced and thermal-induced stresses. Int J Rock Mech Min Sci 46(5):879–895. https://doi.org/10.1016/j.ijrmms.2009.03.002

Bieniawski ZT (1967) Mechanism of brittle failure of rock. Part I. Theory of fracture process. Int J Rock Mech Min Sci Geomech Abstr 4(4):395–406. https://doi.org/10.1016/0148-9062(67)90030-7

Broadbent SR, Hammersley JM (1957) Percolation processes I: crystals and mazes. Math Proc Cambridge Philos Soc 53(3):629–641. https://doi.org/10.1017/S0305004100032680

Cai M, Kaiser PK, Tasaka Y, Maejima T, Morioka H, Minami M (2004) Generalized crack initiation and crack damage stress thresholds of brittle rock masses near underground excavations. Int J Rock Mech Min Sci 41(5):833–847. https://doi.org/10.1016/j.ijrmms.2004.02.001

Cao WG, Zhang S (2005) Study on the statistical analysis of rock damage based on mohr-coulomb criterion. J Hunan Univ: Nat Sci Ed 32(1):43–47. https://doi.org/10.3321/j.issn:1000-2472.2005.01.010

Cao RL, He SH, Wei J, Wang F (2013) Study of modified statistical damage softening constitutive model for rock considering residual strength. Rock Soil Mech 34(6):1652–1660+1667. https://doi.org/10.16285/j.rsm.2013.06.018

Cao AY, Jing GC, Dou LM, Wang GF, Liu S, Wang CB, Yao XX (2015) Damage evolution law based on acoustic emission of sandy mudstone under different uniaxial loading rate. J Min Saf Eng 32(6):923–928+935. https://doi.org/10.13545/j.cnki.jmse.2015.06.009

Chandler NA (2013) Quantifying long-term strength and rock damage properties from plots of shear strain versus volume strain. Int J Rock Mech Min Sci 59:105–110. https://doi.org/10.1016/j.ijrmms.2012.12.006

Chang SH, Lee CI (2004) Estimation of cracking and damage mechanisms in rock under triaxial compression by moment tensor analysis of acoustic emission. Int J Rock Mech Min Sci 41(7):1069–1086. https://doi.org/10.1016/j.ijrmms.2004.04.006

Chen ZH, Tham LG, Yeung MR, Tsui Y, Lee PKK (2002) A study on the peak strength of brittle rocks. Rock Mech Rock Eng 35(4):255–270. https://doi.org/10.1007/s00603-002-0029-x

Chen GQ, Li TB, Zhang GF, Yin HY, Zhang H (2014) Temperature effect of rock burst for hard rock in deep-buried tunnel. Nat Hazards 72(2):915–926. https://doi.org/10.1007/s11069-014-1042-6

Chen GQ, Tang P, Huang RQ, Wang D, Lin ZH, Huang D (2021) Critical tension crack depth in rockslides that conform to the three-section mechanism. Landslides 18:79–88. https://doi.org/10.1007/s10346-020-01471-x

Dong JY, Wang C, Huang ZQ, Yang JH, Xue L (2021) Dynamic response characteristics and instability criteria of a slope with a middle locked segment. Soil Dyn Earthq Eng 150:106899. https://doi.org/10.1016/j.soildyn.2021.106899

Eberhardt E, Stead D, Stimpson B, Read RS (1998) Identifying crack initiation and propagation thresholds in brittle rock. Can Geotech J 35(2):222–233. https://doi.org/10.1139/cgj-35-2-222

Gao L, Gao F, Zhang ZZ, Xing Y (2020) Research on the energy evolution characteristics and the failure intensity of rocks. Int J Min Sci Technol 30(5):705–713. https://doi.org/10.1016/j.ijmst.2020.06.006

Geng JS, Cao LW (2020) Failure analysis of water-bearing sandstone using acoustic emission and energy dissipation. Eng Fract Mech 231:107021. https://doi.org/10.1016/j.engfracmech.2020.107021

Guéguen Y, Chelidze T, Ravalec ML (1997) Microstructures, percolation thresholds, and rock physical properties. Tectonophysics 279(1–4):23–35. https://doi.org/10.1016/S0040-1951(97)00132-7

Hao XJ, Wei YN, Yang K, Su J, Sun YF, Zhu GP, Wang SH, Chen HB, Sun ZW (2021) Anisotropy of crack initiation strength and damage strength of coal reservoirs. Pet Exploration Dev 48(1):211–221. https://doi.org/10.11698/PED.2021.01.20

He MC, Miao JL, Feng JL (2010) Rock burst process of limestone and its acoustic emission characteristics under true-triaxial unloading conditions. Int J Rock Mech Min Sci 47(2):286–298. https://doi.org/10.1016/j.ijrmms.2009.09.003

Hristopulos DT (2003) Renormalization group methods in subsurface hydrology: overview and applications in hydraulic conductivity upscaling. Adv Water Resour 26(12):1279–1308. https://doi.org/10.1016/S0309-1708(03)00103-9

Huang RQ (2012) Mechanisms of large-scale landslides in China. Bull Eng Geol Environ 71(1):161–170. https://doi.org/10.1007/s10064-011-0403-6

Huang SL, Zhong PJ, Ding XL (2021a) Study on characteristic strength anisotropy of layered chlorite schist under uniaxial compression. Chin J Rock Mech Eng 40(S2):3182–3190. https://doi.org/10.13722/j.cnki.jrme.2021.0667

Huang Z, Gu QX, Wu YF, Wu Y, Li SJ, Zhao K, Zhang R (2021b) Effects of confining pressure on acoustic

emission and failure characteristics of sandstone. Int J Min Sci Technol 31(1):963–974. https://doi.org/10.1016/j.ijmst.2021.08.003

Jia Y, Kang YM, Wang D, Zeng DJ, Cao L (2010) Research on critical damage for rock subjected to high confining pressure and temperature-change. J Sichuan Univ: Eng Sci Ed 42(6):79–84. https://doi.org/10.15961/j.jsuese.2010.06.024

Katz O, Reches Z (2004) Microfracturing, damage, and failure of brittle granites. J Geophys Res Solid Earth 109(B1):B01206. https://doi.org/10.1029/2002JB001961

Kong R, Feng XT, Zhang XW, Yang CX (2018) Study on crack initiation and damage stress in sandstone under true triaxial compression. Int J Rock Mech Min Sci 106:117–123. https://doi.org/10.1016/j.ijrmms.2018.04.019

Lemaitre J (1984) How to use damage mechanics. Nucl Eng Des 80(2):233–245. https://doi.org/10.1016/0029-5493(84)90169-9

Li D, Zhou HM (2018) The judgement of unloading points based on crack damage stress and acoustic emission counts. Chin J Undergr Space Eng 14(S1):176–179+219

Li YW, Jia D, Rui ZH, Peng JY, Fu CK, Zhang J (2017) Evaluation method of rock brittleness based on statistical constitutive relations for rock damage. J Pet Sci Eng 153:123–132. https://doi.org/10.1016/j.petrol.2017.03.041

Li XF, Li HB, Liu LW, Liu YQ, Ju MH, Zhao J (2020) Investigating the crack initiation and propagation mechanism in brittle rocks using grain-based finite-discrete element method. Int J Rock Mech Min Sci 127:104219. https://doi.org/10.1016/j.ijrmms.2020.104219

Li K, Yu WJ, Liao Z, Guo HX, Pan B, Khamphouvanh VV, Yang J (2023) A laboratory-testing-based study on mechanical properties and dilatancy characteristics of deeply buried mudstone under different stress loading rates. J China Coal Soc 48(9):3360–3371. https://doi.org/10.13225/j.cnki.jccs.2022.1501

Liang MC, Miao SJ, Cai MF, Huang ZJ, Wang H (2023) Determination method of fatigue strength and precursors of fatigue failure of porous weakly cemented siltstone. J China Coal Soc 48(4):1476–1486. https://doi.org/10.13225/j.cnki.jccs.2022.0313

Liu J, Regenauer-Lieb K (2021) Application of percolation theory to microtomography of rocks. Earth-Sci Rev 214:103519. https://doi.org/10.1016/j.earscirev.2021.103519

Liu ZJ, Zhang CQ, Zhang CS, Gao Y, Zhou H, Chang ZR (2019) Deformation and failure characteristics and fracture evolution of cryptocrystalline basalt. J Rock Mech Geotech Eng 11(5):990–1003. https://doi.org/10.1016/j.jrmge.2019.04.005

Liu LW, Li HB, Li XF (2022) A state-of-the-art review of mechanical characteristics and cracking processes of pre-cracked rocks under quasi-static compression. J Rock Mech Geotech Eng 14(6):2023–2057. https://doi.org/10.1016/j.jrmge.2022.03.013

Lv ZX, Zhao YS, Feng ZJ (2022) Catastrophic failure mechanism of rock masses system and earthquake prediction based on percolation theory. Rock Mech Bull 1(1):100009. https://doi.org/10.1016/j.rockmb.2022.100009

Maheshwari P, Viladkar MN, Venkatesham E (2009) Modified Stanley's approach for statistical analysis of compression strength test data of rock specimens. Int J Rock Mech Min Sci 46(7):1154–1161. https://doi.org/10.1016/j.ijrmms.2009.07.001

Martin CD (1997) Seventeenth Canadian geotechnical colloquium: the effects of cohesion loss and stress path on brittle rock strength. Can Geotech J 34:698–725. https://doi.org/10.1139/cgj-34-5-698

Martin CD, Chandler NA (1994) The progressive fracture of Lac du Bonnet granite. Int J Rock Mech Min Sci 31(6):643–659. https://doi.org/10.1016/0148-9062(94)90005-1

Nakamura AM, Michel P, Setoh M (2007) Weibull parameters of Yakuno basalt targets used in documented high-velocity impact experiments. J Geophys Res 112(E2):02001. https://doi.org/10.1029/2006JE002757

Nicksiar M (2013) Effective parameters on crack initiation stress in low porosity rocks. University of Alberta, Edmonton. https://doi.org/10.7939/R3X59C

Nicksiar M, Martin CD (2012) Evaluation of methods for determining crack initiation in compression tests on low-porosity rocks. Rock Mech Rock Eng 45(4):607–617. https://doi.org/10.1007/s00603-012-0221-6

Ning JG, Wang J, Jiang JQ, Hu SC, Jiang LS, Liu XS (2017) Estimation of crack initiation and propagation thresholds of confined brittle coal specimens based on energy dissipation theory. Rock Mech Rock Eng 51(1):119–134. https://doi.org/10.1007/s00603-017-1317-9

Otsuka M (1972) A simulation of earthquake occurrence. Phys Earth Planet In 6(4):311–315. https://doi.org/10.1016/0031-9201(72)90015-5

Pan XH, Lü Q (2018) A quantitative strain energy indicator for predicting the failure of laboratory-scale rock samples: application to shale rock. Rock Mech Rock Eng 51(9):2689–2707. https://doi.org/10.1007/s00603-018-1480-7

Pathiranagei SV, Gratchev I (2022) Coupled thermo-mechanical constitutive damage model for sandstone. J Rock Mech Geotech Eng 14(6):1710–1721. https://doi.org/10.1016/j.jrmge.2022.02.010

Peng J, Rong G, Cai M, Wang XJ, Zhou CB (2013a) An empirical failure criterion for intact rocks. Rock Mech Rock Eng 47(2):347–356. https://doi.org/10.1007/s00603-012-0355-6

Peng J, Rong G, Zhou CB, Wang XJ, Hou D (2013b) Experimental study of effect of water pressure on progressive failure process of rocks under compression. Rock Soil Mech 34(4):941–946+954. https://doi.org/10.16285/j.rsm.2013.04.024

Peng J, Rong G, Jiang MY (2018) Variability of crack initiation and crack damage for various rock types. Arab J Geosci 11(11):265. https://doi.org/10.1007/s12517-018-3618-z

Pepe G, Mineo S, Pappalardo G, Cevasco A (2017) Relation between crack initiation-damage stress thresholds and failure strength of intact rock. Bull Eng Geol Environ 77(2):709–724. https://doi.org/10.1007/s10064-017-1172-7

Qin SQ, Jiao JJ, Tang CA, Li ZG (2006) Instability leading to coal bumps and nonlinear evolutionary mechanisms for a coal-pillar-and-roof system. Int J Solids Struct 43(25–26):7407–7423. https://doi.org/10.1016/j.ijsolstr.2005.06.087

Qin SQ, Wang YY, Ma P (2010) Exponential laws of critical displacement evolution for landslide and avalanches. Chin J Rock Mech Eng 29(5):873–880

Ranjith PG, Fourar M, Pong SF, Chian W, Haque A (2004) Characterisation of fractured rocks under uniaxial loading states. Int J Rock Mech Min Sci 41:43–48. https://doi.org/10.1016/j.ijrmms.2004.03.017

Ranjith PG, Jasinge D, Choi SK, Mehic M, Shannon B (2010) The effect of CO_2 saturation on mechanical properties of Australian black coal using acoustic emission. Fuel 89(8):2110–2117. https://doi.org/10.1016/j.fuel.2010.03.025

Sahimi M (1996) Linear and nonlinear, scalar and vector transport processes in heterogeneous media: Fractals, percolation, and scaling laws. Chem Eng J Biochem 64:21–44. https://doi.org/10.1016/S0923-0467(96)03103-X

Shao P, He YN (2001) Microcosmic failure detection analysis and critical failure action for brittle rock. Coal Sci Technol 29(7):31–34

Shao P, Xu ZW, Zhang HQ, He YN (2009) Evolution of blast-induced rock damage and fragmentation prediction. Procedia Earth Planet Sci 1(1):585–591. https://doi.org/10.1016/j.proeps.2009.09.093

Shi ZM, Li JT, Wang MX, Tan H, Lin H, Li KH (2023) Effect of temperature on pure mode III fracture behavior and fracture morphology of granite after thermal shock. Theor Appl Fract Mec 127(3):104024. https://doi.org/10.1016/j.tafmec.2023.104024

Taheri A, Zhang YB, Munoz H (2020) Performance of rock crack stress thresholds determination criteria and investigating strength and confining pressure effects. Constr Build Mater 243:118263. https://doi.org/10.1016/j.conbuildmat.2020.118263

Wang B, Zhu JB, Yan P, Huang SL, Wu AQ (2012) Damage strength determination of marble and its parameters evaluation based on damage control test. Chin J Rock Mech Eng 31(S2):3967–3973

Wang CP, Chen L, Liu JF, Liu J (2015) Experimental characterisation of thermo-mechanical coupling properties of Beishan granite. Eur J Environ Civ Eng 19(sup1):s29-s42. https://doi.org/10.1080/19648189.2015.1064618

Wang HT, He MM, Zhang ZQ, Zhu JW (2022) Determination of the constant m_i in the Hoek-Brown criterion of rock based on drilling parameters. Int J Min Sci Technol 32(4):747–759. https://doi.org/10.1016/j.ijmst.2022.06.002

Wang HT, He MM, Zhao JB, Zhang YH, Yang BB (2023) Cutting energy characteristics for brittleness evaluation of rock using digital drilling method. Eng Geol 319(4):107099. https://doi.org/10.1016/j.enggeo.2023.107099

Wei SS, Shen JS, Yang WY, Li ZL, Di SH, Ma C (2019) Application of the renormalization group approach for permeability estimation in digital rocks. J Petrol Sci Eng 179:631–644. https://doi.org/10.1016/j.petrol.2019.04.057

Weibull W (1951) A statistical distribution function of wide applicability. J Appl Mech 18:293–297. https://doi.org/10.1115/1.4010337

Xie SJ, Lin H, Duan HY (2023) A novel criterion for yield shear displacement of rock discontinuities based on renormalization group theory. Eng Geol 314:107008. https://doi.org/10.1016/j.enggeo.2023.107008

Xue L, Sun Q, Wang YY, Wang SW, Li GL, Pan XH (2013) Study on the critical stress state of brittle failure of rock based on renormalization group theory. J Basic Sci Eng 21(4):710–724. https://doi.org/10.3969/j.issn.1005-0930.2013.04.013

Xue L, Qin SQ, Sun Q, Wang YY, Lee LM, Li WC (2014a) A study on crack damage stress thresholds of different rock types based on uniaxial compression tests. Rock Mech Rock Eng 47(4):1183–1195. https://doi.org/10.1007/s00603-013-0479-3

Xue L, Qin SQ, Sun Q, Wang YY, Qian HT (2014b) A quantitative criterion to describe the deformation process of rock sample subjected to uniaxial compression: From criticality to final failure. Physica A 410:470–482. https://doi.org/10.1016/j.physa.2014.05.062

Yang SQ, Liu XR (2012) Experimental investigation on dilatancy behavior of marble with pre-existing fissures under different confining pressures. Chin J Geotech Eng 34(12):2188–2197

Yang SJ, Zeng S, Wang HL (2005) Experimental analysis on mechanical effects of loading rates on limestone. Chin J Geotech Eng 27(7):786–788

Yang YM, Ju Y, Mao LT (2014) Growth distribution laws and characterization methods of cracks of compact sandstone subjected to triaxial stress. Chin J Geotech Eng 36(5):864–872. https://doi.org/10.11779/CJGE201405008

Yang BC, Xue L, Wang MM (2018) Evolution of the shape parameter in the Weibull distribution for brittle rocks under uniaxial compression. Arab J Geosci 11:321. https://doi.org/10.1007/s12517-018-3689-x

Yang BC, Qin SQ, Xue L, Chen HR (2021) The reasonable range limit of the shape parameter in the weibull distribution for describing the brittle failure behavior of rocks. Rock Mech Rock Eng 54(6):3359–3367. https://doi.org/10.1007/s00603-021-02414-1

Yang BC, Zhao W, Duan YT (2022a) Critical damage threshold of brittle rock failure based on renormalization group theory. Geomech Geophys Geo-Energ Geo-Resour 8(5):135. https://doi.org/10.1007/s40948-022-00441-y

Yang BC, Bai JX, Duan YT Wang ZP (2022b) The unlocked mechanism and instability prediction of a typical locked-segment-type slope in China: the Chana landslide. B Eng Geol Environ 81(12):493. https://doi.org/10.1007/s10064-022-03001-6

You S, Li F, Sun JC, Ji HG, Wang HT (2021) Experimental study on hydraulic failure mechanism and energy storage characteristics of deep granite. J Cent South Univ Sci Technol Ed 52(8):2839–2848. https://doi.org/10.11817/j.issn.1672-7207.2021.08.029

Zhang LM, Ren MY, Ma SQ, Wang ZQ, Guo Q (2016) Study on the physical-mechanical parameters of marble under different stress paths. Chin J Undergr Space Eng 12(5):1288–1293+1325

Zhang CQ, Lu JJ, Chen J, Zhou H, Yang FJ (2017) Discussion on rock burst proneness indexes and their relation. Rock Soil Mech 38(5):1397–1404. https://doi.org/10.16285/j.rsm.2017.05.022

Zhang XP, Lü GG, Zhang Q, Liu QS, Li WW, Xu JL (2020) Uniaxial compression test for three stress thresholds of siliceous siltstone. J Eng Geol 28(3):441–449. https://doi.org/10.13544/j.cnki.jeg.2019-085

Zhang JB, Zhang XH, Chen W, Huang Z, Du RH (2022) A constitutive model of freeze–thaw damage to transversely isotropic rock masses and its preliminary application. Comput Geotech 152(1):105056. https://doi.org/10.1016/j.compgeo.2022.105056

Zhao YL, Liu Q, Liu H, Liao J, Chang L, Tan T, Song F (2021) Triaxial compression and acoustic emission tests on single cracked limestone and compression-shear fracture model under hydraulic-mechanical coupling action. J China Coal Soc 46(12):3855–3868. https://doi.org/10.13225/j.cnki.jccs.2021.0367

Zhou HW, Wang ZH, Ren WG, Liu ZL, Liu JF (2019) Acoustic emission based mechanical behaviors of Beishan granite under conventional triaxial compression and hydro-mechanical coupling tests. Int J Rock Mech Min Sci 123:104125. https://doi.org/10.1016/j.ijrmms.2019.104125